39th IAHR WORLD CONGRESS GRANADA, SPAIN 2022 From Snow to Sea 19-24 June 2022

Proceedings of the 39th IAHR World Congress
19–24 June 2022, Granada, Spain
doi://10.3850/IAHR-39WC2521716X2022576

Observations of hydrodynamics and sediment transport in the Orinoco River

Carlo Gualtieri[(1)], Santiago Yepez[(2)], Mauricio Bermudez[(3)] and Alain Laraque[(4)]

[(1)] University of Napoli Federico II, Napoli, Italy, e-mail carlo.gualtieri@unina.it
[(2)] Universidad de Concepción, Concepción, Chile, e-mail syepez14@gmail.com
[(3)] Universidad Pedagógica y Tecnológica de Colombia, Sogamoso-Boyacá, Colombia, e-mail maberce@gmail.com
[(4)] GET, UMR CNRS / IRD / UPS, Toulouse, France, e-mail alain.laraque@ird.fr

Abstract

The Orinoco River has the third largest discharge in the world, with an annual mean flow of 37600 m^3/s at the outlet to the Atlantic Ocean. Several field studies were carried out within the HYBAM Program to characterize hydrodynamics and sediment transport in the reach of the Orinoco River close to the city of Ciudad Bolivar (Venezuela). The studies were performed in low, medium, and high flow conditions. During this field campaign, Acoustic Doppler Velocity Profiling (ADCP) was used as well as water sampling for the measurement of total suspended sediment (TSS).
Surface sedimentary fluxes were ranging from 68 to 113 Mton/year for the bimodal sedimentological regime in the hydrological station at Ciudad Bolivar, marked by two TSS peaks respectively, before and after the maximum discharge peak. The ADCP measurements gained a comprehensive characterization of the basic hydrodynamics and sediment transport parameters in that reach as well as their variation in different flow conditions during the hydrological year. Large differences in discharge, flow velocities. Finally, bed shear stress distribution identified dominant transport mode and maximum suspended grain size, being in the range order of fine sands and very fine sands in medium/high flow and low flow conditions, respectively.

Keywords: Orinoco River; Field study, ADCP, River hydrodynamics, Sediment transport

1. INTRODUCTION

World's large rivers and their floodplains have been historically key locations for the establishment of human civilization. Yellow River, Indus, Nile, Tigris and Euphrates have been the cradle of old civilizations (Macklin and Lewin, 2015). At present time, large rivers are increasingly attracting the attention within the social media and the scientific community as they support huge population, represent some of the most diverse ecosystems of our planet and are threatened by several anthropogenic stressors, including large-scale damming, rapid urbanization, sea-level change, deforestation, hydrological change, pollution, introduction of non-native species and sediment mining (Blum, 2007; Best, 2018). The definition of a "large river" is still controversial as it could relate to the river discharge, channel size, distinctive floodplain/channel styles and hydrologic connectivity as well as to geologic control by structure or tectonics (Potter, 1978; Junk et al., 1989; Latrubesse et al., 2005; Gupta, 2007; Wohl, 2007). Nevertheless, the size of a river is mostly defined in term of (1) the area of the drainage basin, (2) the length of course, (3) the water discharge and (4) the volume of sediment in transport (Potter, 1978; Gupta, 2007). Latrubesse (2008) proposed to define a *large river* and *mega-river* as having an average annual discharge Q_{avg} larger than 1000 m^3/s and 17000 m^3/s, respectively. Following this definition, there are 11 mega-rivers on the Earth: Amazon, Congo, Orinoco, Yangtze, Madeira, Negro, Brahmaputra, Japurá, Paraná, Mississippi and Yenisei. The *mega rivers* share several common characteristics. They are predominantly sand-bed channels, with low gradients (<10 cm/km), flow depths up to 25-50m or more, individual channels with large widths W (1–10 km) and width to depth ratios W/h (W/h=30–200), low Froude numbers, that are typically <0.3 (Amsler and Garcia, 1997) and a wide range of roughness scales associated with alluvial bedforms including ripples, dunes, and unit bars (Latrubesse, 2008). They also present *anabranching* channel patterns, i.e. with a system of multiple channels that divide and rejoin, where individual branches between permanent islands have a range of patterns: straight, meandering, braided, wandering or anastomosing (Latrubesse, 2008; Ashworth and Lewin, 2012; Nicholas et al., 2013).

If in recent years *mega rivers* have received a significant attention within the Earth Sciences community (Ashworth and Lewin, 2012; Lewin and Ashworth, 2014; Best and Darby, 2020), few comprehensive studies focused on hydrodynamics and sediment transport in such very large riverine systems are available. Getirana and Paiva (2013) presented a map of river hydrodynamic in the Amazon Basin using a classification method based on the analysis of Saint-Venant equation terms, while Nicholas et al. (2012, 2013) simulated bar and

island morphodynamics in Paraná, Japurá and Jamuna- Brahmaputra. A limited number of field studies were conducted at *mega rivers* confluences, such as Jamuna/Ganges-Brahmaputra (Best and Ashworth, 1997), Paraná-Paraguay (Lane et al., 2008), Negro/Solimões (Gualtieri et al., 2018; Ianniruberto et al., 2018; Gualtieri et al., 2019) and Yangtze/Poyang Lake (Yuan et al., 2021), and diffluence-confluence units, which are characteristic of the anabranching pattern of most *mega rivers*, such as in Paraná River (Parsons et al., 2007; Szupiany et al., 2009, 2012), Yangtze River (Liu et al., 2020) and Mississippi River (Wang et al., 2020). Among the *mega rivers*, the Orinoco is one of the less investigated and studies about hydrodynamics and sediment transport are almost completely lacking. Only recently, Yepez et al. (2018) studied the dynamics and evolution of sand waves and bars in the lower Orinoco quantifying the volume (erosion vs. accretion) of a mid-channel bar with dunes using field data.

The paper presents the results from a series of field studies conducted from 2012 to 2017 in low, medium and high flow conditions in a reach of the Orinoco River near the city of Ciudad Bolivar, where is located one of the eight major bedrock control points along the lower Orinoco River (Warne et al., 2002). The main objective of this study is to present and discuss the main hydrodynamics and sediment transport features and their changes observed during the field studies providing a comprehensive report of such characteristics in the Orinoco River.

2. ORINOCO RIVER. FIELD SITE, INSTRUMENTATION AND DATA POST-PROCESSING

2.1 Orinoco River

The Orinoco River has the third largest discharge in the world, with an annual mean flow of 37600 m^3/s at the outlet to the Atlantic Ocean. It originates from Cerro Delgado–Chalbaud, at 1047 m above the sea level and its main channel is 2140 km (Silva León, 2005) long from the Brazilian border to its mouth in the Atlantic Ocean. The Orinoco River Basin covers about 1.1×10^6 km² being located 70% and 30% in Venezuela and Colombia, respectively (Silva León, 2005) (Figure 1). The basin has three large geographic zones: (1) the Andes and Caribbean Coastal Ranges, where most suspended sediments originate; (2) the Llanos (floodplain area), which are crossed by all major tributaries coming from the Andes and (3) the Precambrian Guiana Shield from which drains predominantly black water with very low suspended sediment content (Warne et al., 2002; Laraque et al., 2013; Yepez et al., 2018). Rainfall rate in the Orinoco River basin and Delta typically ranges from 120 to 360 mm/year, while temperature is uniform in the lowland regions, ranging from 25 to 28 °C (Warne et al., 2002). This marked range between wet and dry season results in large fluctuations in discharge and stage, that are typically 10-12 m and even 16 m in the lower Orinoco (Yepez et al., 2018).

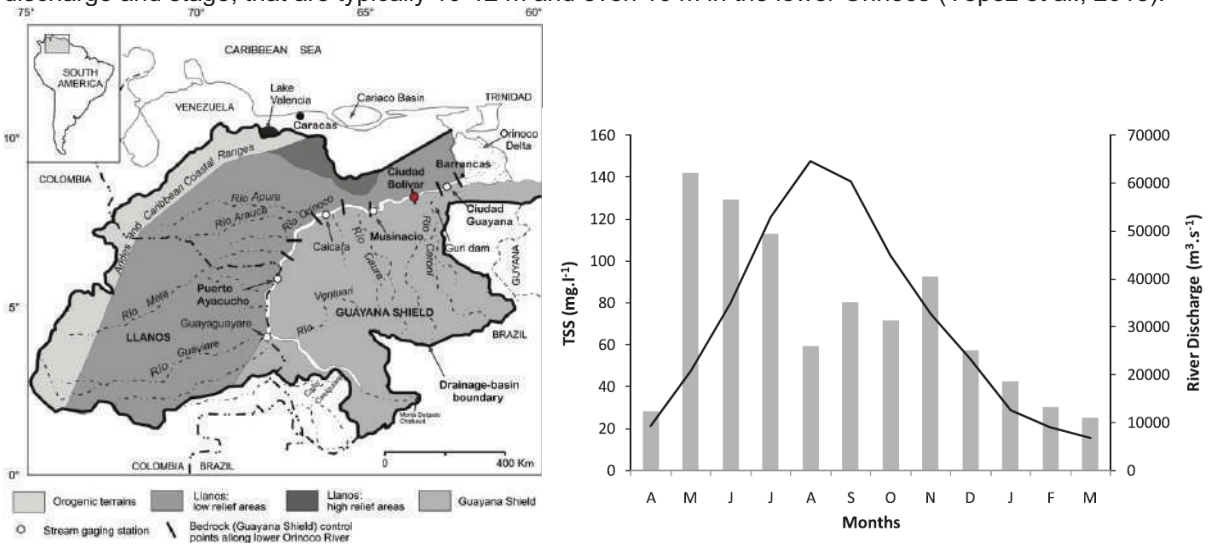

Figure 1. (Left) The Orinoco River and (right) mean monthly discharge (line) and mean monthly sediment concentration (histogram) at Ciudad Bolivar from 2005 to 2010 (from Laraque et al., 2013)

2.2 Field site and instrumentation

In the lower Orinoco, while water discharge variations are unimodal, two peaks in sediment loads are typically observed, with a maximum during rising flood discharge (April–May), a minimum during peak water discharge (August–September), and a secondary maximum during the recession of flood discharge (October–November) (Figure 1). The amplitude between the low and high waters is about 16 m. The sedimentological

regime is bimodal (Laraque et al., 2013). As flooding starts, the sparsely vegetated sediment deposited during the previous late flood stage and those redistributed by winds during the dry season, are easily entrained. Later, as discharge peak is approaching, the water levels in the main channel exceed those of the tributaries from the low gradient Llanos causing tributary flood water to pond at the confluences and temporary sediments deposition in the tributaries. As the water levels in the main channel decrease, a portion of the sediment deposited at the confluences of the main tributaries is remobilized, causing the second peak in sediment load (Nordin and Pérez-Hernández, 1989; Meade et al., 1990; Warne et al., 2002).

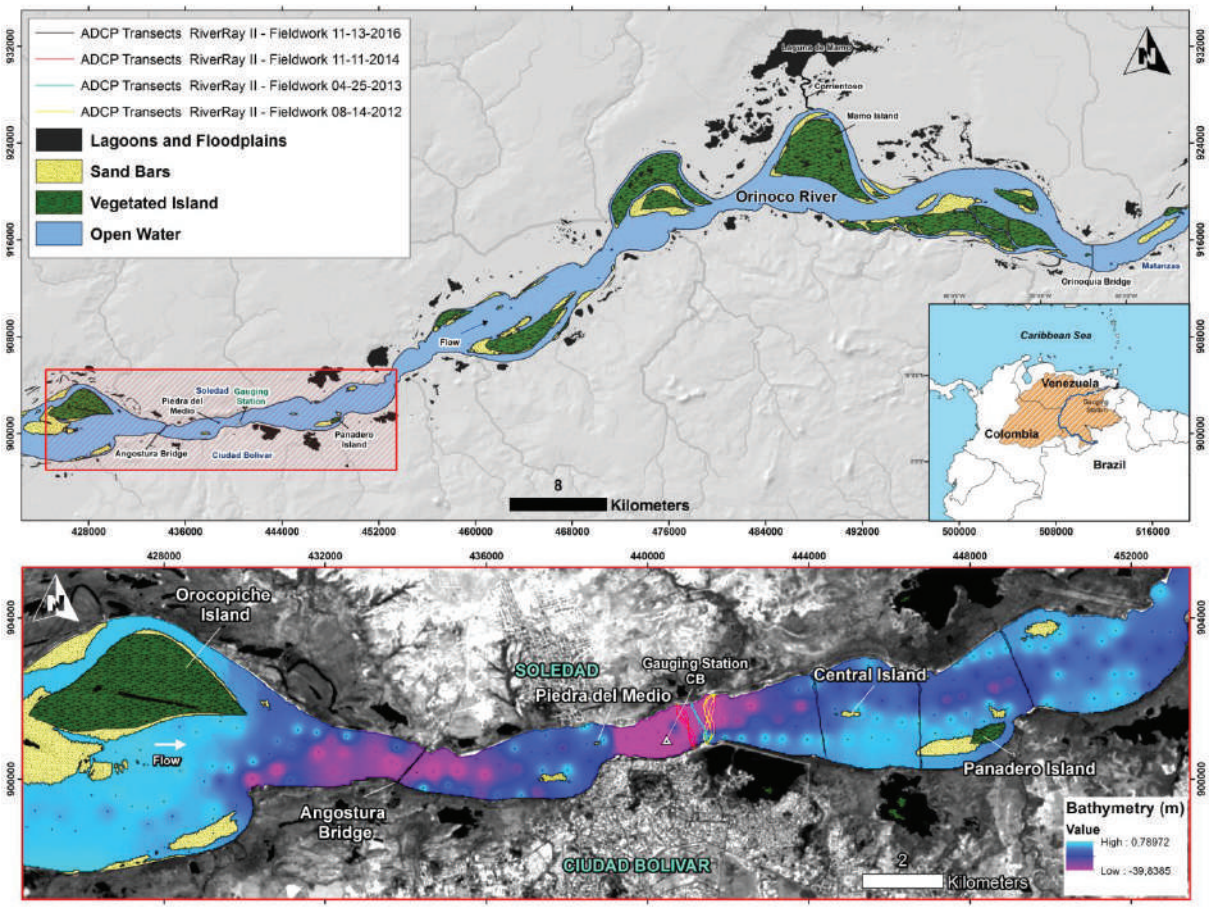

Figure 2. Study area (red square) in the contraction / expansion channel of the lower Orinoco River in Ciudad Bolívar. The bathymetry is superimposed on a Landsat-8 OLI image of January 11, 2016

Flow conditions were surveyed in a about 8.5 km reach of the lower Orinoco River from 2012 to 2016. This section of the river is located between *Piedra del Medio* Island nearby to Ciudad Bolivar town and a downstream sector near to the *Panadero* Island. 4 km upstream Angostura bridge, the width of the main channel varies from 7-8 km, while in the narrowest part of the funnel between Ciudad Bolivar and Soledad town the width reach a 900 m approximately (Figure 2), marked by the presence of bedrock controls, being one of the most important the *Piedra del Medio* island. This reach is characterized by numerous sand bars and islands that divide the flow into several channels (López and Perez-Hernandez, 1999).

In that reach, daily water stage records and discharges are available at Ciudad Bolivar gauging station since 1926, being the most complete flow measurement station in the Orinoco basin so far. The data has been registered by the Venezuelan water agency-INAMEH with the support of Institute of Fluids Mechanics in the Central University of Venezuela (UCV-IMF) using traditional gauging techniques with current-meters before 2010, and Acoustic Doppler Current Profiler (ADCP) thereafter. As part of this study, 6 complete hydrological cycles were studied from data collected at Ciudad Bolivar between the years 2012 to 2017.

A detailed series of acoustic Doppler current profiler (ADCP) transects were carried out from August 14, 2012 to November 11, 2016 at 6 different locations near Ciudad Bolivar (Figure 2). The surveys were part of the Ecos-Nord V14U01 Project and SO Hybam Program. A RiverRay II (RD Instruments, 2017) integrated with the Trimaran float was applied. The transects carried out in 2012/2014 were located at the end of channel contraction, while in 2016 the data were collected upstream/downstream of Panadero Island and farther downstream in a bend (Figure 2).

Table 1 lists the measured discharge, channel width and the distance from the *Piedra del Medio* island. In each cross-section, several measurements were carried out (from 2 to 4 transects by section). An average of 20–25 minutes was required for each one of the 19 transects having a width from 1 Km to 2.3 km. The ADCP measurements were collected in low, medium and high flow conditions with a discharge of approximately 10000, 35000, and 65000 m³/s, respectively.

Table 1. Transects analysed in the Lower Orinoco River during the 2012/2016 fields studies

Name	Date	Transects	Distance (m)	Q (m³/s)	W (m)	Flow conditions	Comments
H1	14/08/2012	5	2675	64821	1253	High	ADCP, TSS
L1	25/04/2013	4	2475	10515	978	Low	ADCP, TSS
M1	11/11/2014	4	2155	39722	1200	Medium	ADCP, TSS
M2	13/11/2016	2	5435	33908	2037	Medium	ADCP, TSS
M3	13/11/2016	2	7910	34501	2294	Medium	ADCP, TSS
M4	13/11/2016	2	10670	34214	2053	Medium	ADCP, TSS

Legend: Q = discharge; W = transect width

In addition, from January 2012 to December 2017, the HYBAM observation service (http://www.so-hybam.org/index.php /eng/Data) collected at Ciudad Bolivar station, a total of 136 surface water samples. 38 of them were collected with a frequency of 10 days until August 2013, while, later, 98 were taken with a lower frequency of 1-2 times per month. Sampling was carried out at channel centerline. For the determination of total suspended sediments (TSS) concentration, a unit of frontal filtration tied to a vacuum pump was used in the water samples, including filters of cellulose acetate of 0.45 µm of porosity. After filtration, the filters are dried for 24h at 60° C and weighed. TSS concentration was calculated as the difference between the weight of the filter after and before filtration divided by the volume of water collected.

2.3 Data post-processing

Following Laraque et al. (2013) it was assumed that a simple sample in the center of the cross section is representative of the entire section of Ciudad Bolivar. Therefore, surface TSS load (Ton/yr) was calculated as:

$$TSS = \left[\sum_{1}^{n} \frac{(C_i * Q_j)}{Q_m}\right] \quad [1]$$

where n is number of analysis during the months, C_i: is the instantaneous concentration and Q_j and Q_m are the daily and monthly water discharge.

The analysis of the ADCP data first gained basic geometric and hydrodynamics parameters, while further information was derived using the Velocity Mapping Tool software (Parsons et al., 2013).

Any deviation from the assumption of a uniform velocity distribution over the cross-section is accounted for using two coefficients, the Coriolis coefficient α for kinetic energy and the Boussinesq coefficient β for momentum (Chanson, 2004). They must be applied in any analysis or computation based upon the energy and momentum principle, respectively, if average velocity is used. If water density is constant, they are defined as:

$$\alpha = \frac{\int_A V^3 \, dA}{V_{avg}^3 \, A} \quad [2]$$

$$\beta = \frac{\int_A V^2 \, dA}{V_{avg}^2 \, A} \quad [3]$$

where V_{avg} is the average cross-sectional velocity and V is the effective velocity in any point. In this study, the depth-averaged velocity was applied to represent the distribution of the velocity in the river cross-section.

In alluvial channels friction is related both to the grain resistance and to the form of bedforms. Hence, the total friction is the sum of these terms as (Chanson, 2004):

$$\tau_b = \tau_b' + \tau_b'' \quad [4]$$

where τ'_b and τ''_b are the skin friction shear stress and the form-related shear stress, respectively.

The approach proposed by Sime et al. (2007) for moving boat ADCP profiling was applied to estimate skin friction shear stress. They demonstrated that a quadratic-stress approach based upon the depth-averaged velocity and a zero-velocity height related to the bed grain size is more precise than the estimation based on the mean velocity and near-bed velocity, which are affected from uncertainties in the measurement of bed elevation and near-bed velocity. Hence, the skin friction shear stress can be calculated as:

$$\tau_b' = \rho C_d V_{depth-avg}^2 \quad [5]$$

where C_d is the drag coefficient, which was obtained as:

$$C_d = \frac{k^2}{ln^2(h/e\ z_0)} \quad [6]$$

where κ is the von Kármán constant, e is the Euler number and z_0 is the zero−velocity height above the bed.

Sime et al. (2007) assumed that z_0=0.1 d_{84}, where d_{84} is bed grain diameter such that 84% of diameters are finer. Bed sediment sampling provided a d_{84} of 0.341 mm (medium sand). Using the above method, the skin friction stress, which is related to the *bed load mode*, was calculated. The different modes of transport were determined using the *Rouse number Ro*:

$$Ro = \frac{w_s}{\kappa u^*} \quad [7]$$

where w_s is the fall (settling) velocity of the particles. If the Rouse number varies between 0.8 and 2.5, the transport is within the *suspended load* mode; when it goes beyond 2.5, the transport is as *bed load* (Bombardelli and Moreno, 2012). Finally, the skin friction shear stress can also be applied to approximate the maximum particle size in suspension (Trevethan and Aoki, 2009):

$$d_{ss} = \sqrt{\frac{18\rho v \cdot 0.8 \cdot \sqrt{\tau_b/\rho}}{g(\rho_s - \rho)}} \quad [8]$$

where ρ_s is the particle density and v is the water kinematic viscosity.

3. RESULTS

3.1 Surface sedimentary loads and TSS concentration

TSS concentration and the estimated surface sedimentary loads in the Orinoco River at Ciudad Bolivar from 2012 to 2017 are listed in Table 2. TSS concentration was in the range from 12 to 277 mg/L, while surface sediment loads were from 68 to 113 Mton/year.

Table 2. Annual sediment load, weighted by the mean monthly flow at Ciudad Bolivar station

Year	TSS Mean (mg/L)	TSS max (mg/L)	TSS min (mg/L)	N° samples	Surface Sediment Load (*) (Mton/yr)	Q_{mean} (m^3/s)	Q_{max} (m^3/s)	Q_{min} (m^3/s)
2012	77.7	189.2	21.1	36	88	37090	73483	8396
2013	74.8	213.6	18.2	28	68	32126	62271	5516
2014	89.8	170.0	18.9	10	100	30536	67256	5093
2015	89.0	203.0	29.0	14	91	28531	67183	6434
2016	109.2	277.0	12.0	26	113	34239	73938	4258
2017	97.0	210.9	23.3	24	103	34302	77315	7520
mean	**90**	**211**	**20**	**23**	**94**	**32804**	**70241**	**6203**
max	**109**	**277**	**29**	**36**	**113**	**37090**	**77315**	**8396**
min	**75**	**170**	**12**	**10**	**68**	**28531**	**62271**	**4258**
min/max	**0.7**	**0.6**	**0.4**	**0.3**	**0.6**	**0.8**	**0.8**	**0.5**

(*) Sediment load weighted by mean monthly flow

3.2 Basic hydrodynamics parameters

The ADCP was used to measure three-dimensional water velocities over the water depth along the transect, as well as water temperature near the surface and backscatter intensity, which after a proper calibration could be related to suspended sediment concentration (Szupiany et al., 2009). The analysis of the ADCP data first gained the basic hydrodynamics parameters such are area, wetted perimeter, hydraulic ratio, average/median water depth, aspect ratio, cross-sectional average velocity, and average/median depth-averaged velocity. Some of these parameters are listed in Table 3, in which the median value from each field study is presented.

Table 3 shows that large differences in discharge and flow velocities were observed in each survey according to the hydrological cycle. From low flow to high flow conditions, the maximum depth-averaged velocity at the end of channel contraction increased from 1.07 to 2.77 m/s, while in the reach around Central Island was of about 1.75-1.95 m/s. In the contracted channel, the cross-sectional velocity raised from 0.4 to 1.5 m/s from low flow to high flow conditions. Furthermore, from low flow to high flow conditions the contracted channel increased in depth, from 25 to 34 m and in width from 950 to 1250 m, whereas downstream about Panadero Island the depth was in the order of 10-16 m and the width of 2000 m. Thus, the channel aspect ratio after the expansion raised from 37-45 to 117-155. Finally, some change in the median of the flow direction was observed from medium to both low and high flow conditions in the contracted channel. It should be noted that previous studies (Mora et al., 2009; Laraque et al., 2013) have identified the presence of strong rapids and high turbulence at the entrance of the contraction, in a reach that is considered as a bedrock control.

Table 3. Main flow properties of the Orinoco River at Ciudad Bolivar during the 2012/2016 field studies

Name	Date	Flow conditions	Q (m^3/s)	A (m^2)	W (m)	h_{med} (m)	W/h_{rect} (-)	V_{avg} (m/s)	$V_{depth-avg}$ (m/s)	Dir (°)	V_{max} (m/s)
H1	14/08/2012	High	64821	41783	1253	34.7	37	1.52	1.28	81	2.77
L1	25/04/2013	Low	10515	24563	978	25.2	39	0.43	0.46	83	1.07
M1	11/11/2014	Medium	39722	32217	1200	25.5	45	1.23	1.24	91	2.05
M2	13/11/2016	Medium	33908	33273	2037	16.5	125	1.02	1.11	90	1.74
M3	13/11/2016	Medium	34501	33993	2294	10.5	155	1.01	1.02	84	1.95
M4	13/11/2016	Medium	34214	35948	2053	16.0	117	0.95	0.98	74	1.75

Legend: Q = discharge; A = cross-sectional area; h_{med} = median depth; W/h_{rect} = aspect ratio; V_{avg} = cross-section velocity (Q/A); $V_{depth-avg}$ = median of the depth-averaged velocity; Dir = median of flow direction degrees from North; V_{max} = maximum depth-averaged velocity

Fig.3 shows the depth-averaged velocity data (magnitude and direction) collected at each transect. The figure was plotted using the VMT (Velocity Mapping Tool) software (Parsons et al., 2013). Large depth-averaged velocities were observed at the contracted channel, while lower velocities were in the reach immediately upstream of the Central Island, where the flow split in two parts. Downstream of this island the flow adjusted its magnitude/trajectory following the change in water depth and the meandering path of the channel.

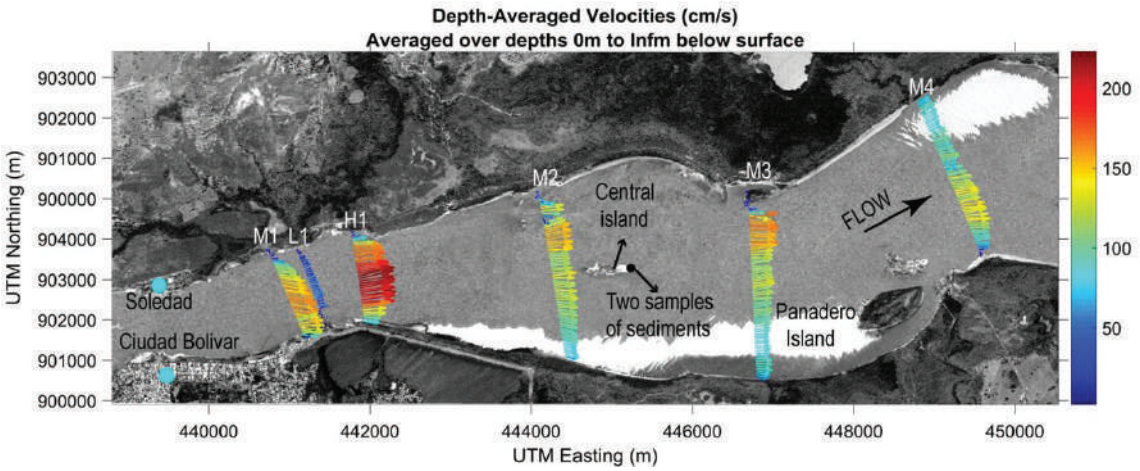

Figure 3. Depth-averaged velocities of ADCP transects collected in 2012-2016 in the lower Orinoco near Ciudad Bolivar

Averaging from 2 to 5 repeated transects, the flow at each location was further investigated using VMT software. Figures 4 and 5 show the cross-sectional distribution of velocity magnitude with secondary flow vectors calculated with Rozovski method at transects H1 and L1, respectively, that were located upstream of channel expansion. They were measured in high and low flow conditions, respectively. In high flow conditions the velocity magnitude reached even almost 3.00 m/s, while in low flow the velocity in the central part of the cross section was lower than 0.80 m/s. Fig.6 presents the velocity magnitude at transect M3, which was located downstream of the Central Island and upstream of Panadero Island, during medium flow conditions. Velocity magnitude was up to 2.0 m/s on the left side and much lower at the right side, where water depth was even lower than 5 m.
In all transects, intense secondary flow was identified, mostly in the central part of the cross-section.

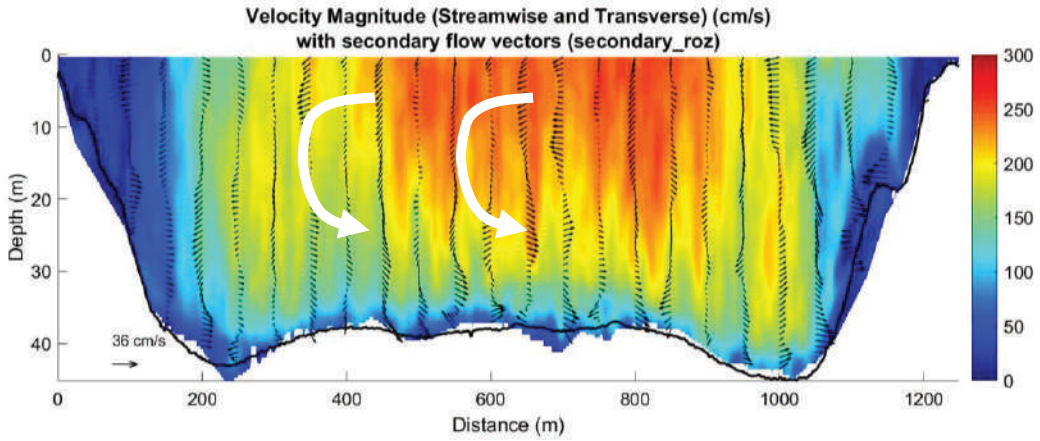

Figure 4. Cross-sectional distribution of velocity magnitude with secondary flow vectors – Transect H1

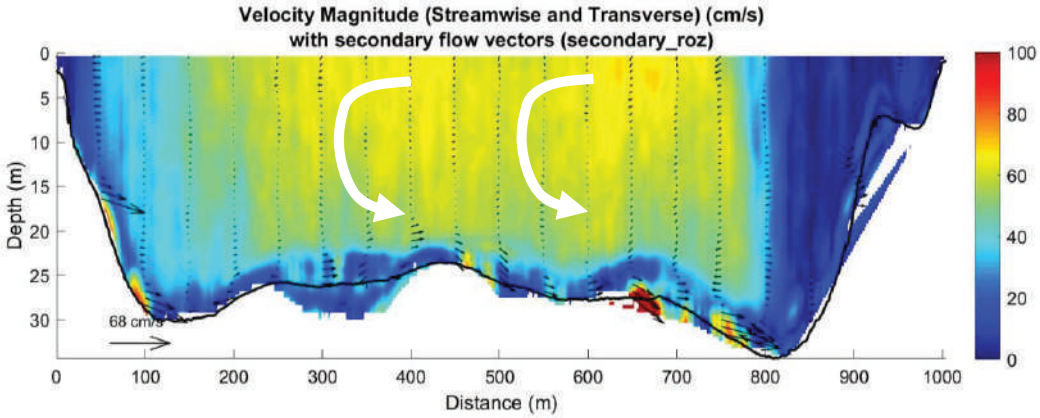

Figure 5. Cross-sectional distribution of velocity magnitude with secondary flow vectors – Transect L1

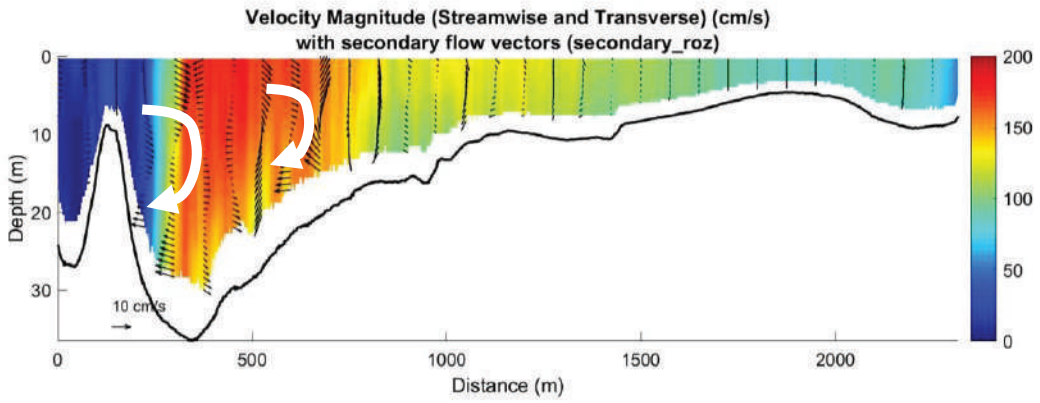

Figure 6. Cross-sectional distribution of velocity magnitude with secondary flow vectors – Transect M3

Theoretical values for α and β can be derived from the power law and the logarithmic law for velocity distribution in wide channels. For turbulent flow in a straight channel having a rectangular, trapezoidal, or circular cross section, α is usually less than 1.15 (Henderson, 1966), whereas for natural channels Coriolis and Boussinesq coefficients are typically in the range from 1.15 to 1.50 and from 1.05 to 1.17 (Chaudry, 2008). For example. in the Amazon Basin, in low flow conditions values of α of 1.41 and 1.27 were observed in the Negro and Solimões rivers, whereas the Boussinesq coefficient was 1.23 and 1.10, respectively.

Fig. 7 shows the distribution of α and β in the reach of the Orinoco River considered in this study. First, in the channel contraction both coefficients have values larger than those reported in natural channels. Second, for β (Figure 4B), the lowest was the discharge, the highest was the coefficient. This indicates that, high flow conditions (Q=64821 m³/s) tended to homogenize the velocity distribution, while for the falling waters stage (Q=10515 m³/s) the distribution of depth-averaged velocity exhibited large variations respect to the average cross-sectional velocity. Third, in medium flow conditions, both coefficients were larger in the channel expansion than in the contracted channel. Immediately downstream of the Central Island (Figure 3 - Transect M3) the coefficients increased having the largest value and then decreased (Figure 3 - Transect M4). This suggests an effect of variation in channel width and of the island on the uniformity of velocity distribution.

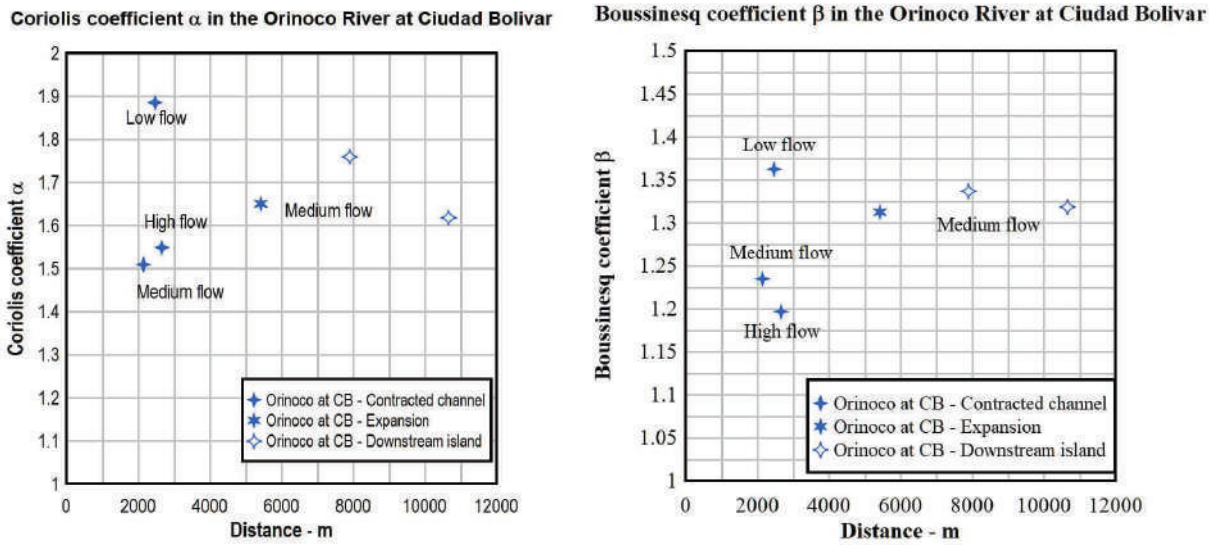

Figure 7. Longitudinal distribution of α and β coefficients.

3.3 Sediment transport parameters

One of the objectives of the field campaigns was to study the interaction between hydrodynamics and sediment transport as well as morphodynamics in the lower Orinoco. This transport is possible as the intensity of the water flow is strong enough to move the finer particles away from the bed and to carry them along the current, while heavier particles are harder to be moved and either remain on the bed, move close to the bed, sliding or rolling, or deposit once moved, i.e. saltation (Bombardelli and Moreno, 2012).

Table 4. Main sediment transport properties in the Lower Orinoco River during the 2012/2016 field studies

Name	Date	Q (m³/s)	τ'_b (Pa)	u* (m/s)	Ro	d_{ss} (mm)
H1	14/08/2012	64821	1.60	0.040	1.90	0.181
L1	25/04/2013	10515	0.22	0.015	5.10	0.109
M1	11/11/2014	39722	1.72	0.042	1.84	0.182
M2	13/11/2016	33908	1.44	0.038	2.01	0.174
M3	13/11/2016	34501	1.30	0.036	2.11	0.170
M4	13/11/2016	34214	1.17	0.034	2.23	0.165

Legend: Q = discharge; τ'_b = bed shear stress; u* = shear velocity; Ro = Rouse number; d_{ss} = maximum suspended grain size

Table 4 lists the median values for each transect of the main sediment transport parameters. They show a large variation in bed shear stresses from the low flow to the medium/high flow conditions. The median

shear stress was from 0.22 to 1.60 Pa in low and high flow conditions, respectively. The Rouse number indicated that in medium and high flow conditions the dominant mode for d_{84} was the *suspended load* mode, while in low flow conditions it shifted to the *bed load* mode. The maximum suspended grain size d_{ss} was in the order of fine sands and very fine sands in medium/high flow and low flow conditions, respectively. Note that these values of *Ro* and d_{ss} should be considered as an upper and lower boundary, respectively, because they were based only upon the skin friction shear stress and not upon the total stress τ_b in [4].

4. CONCLUSIONS

Hydrodynamics and sediment transport in the Orinoco River, which has the third largest discharge in the world, have been rarely investigated. The present study summarizes the results of several field surveys carried out from 2012 to 2016 within the HYBAM Program in the Lower Orinoco River close to the city of Ciudad Bolivar (Venezuela). In that reach, the channel width rapidly expands from 900 m to more than 2.0 km.

The studies were performed in low, medium, and high flow conditions using ADCP and water sampling for the measurement of total suspended sediment (TSS). Surface sedimentary load was estimated to be in the range from 68 to 113 Mton/year. Large differences in discharge and flow velocities were observed in each survey according to the hydrological cycle. In the contracted channel, from low to high flow conditions, the maximum depth-averaged velocity and the cross-sectional velocity increased from 1.07 to 2.77 m/s and from 0.4 to 1.5 m/s, respectively. Farther downstream, flow patterns and magnitude were likely affected from the two islands, i.e. Central Island and Panadero Island, as well as from the meandering path of the channel.

The analysis of cross-sectional flow patterns revealed large variation in velocity distribution among the different flow conditions and intense secondary flows. Coriolis and Boussinesq coefficients exhibited an inverse relationship with discharge and were larger in the channel expansion than in the contracted channel. Finally, bed shear stress distribution identified dominant transport mode and maximum suspended grain size, being the latter in the range order of fine sands and very fine sands in medium/high flow and low flow conditions, respectively.

5. ACKNOWLEDGEMENTS

The field campaigns on the Orinoco River were supported by the SO-HYBAM project and ECOSNord/Fonacit (V14U01), as well as by the Bolivarian National Armada of Venezuela and COEA-IVIC laboratory. The second author was financially supported by IRD-ARTS Grant 2017-2018 and Venezuela's Fundayacucho Grant No. E-223-14-2014-2. The third author acknowledge the financial support from UPTSC SGI-DIN-3104.

6. REFERENCES

Ashworth, P.J., Lewin, J. (2012). How do big rivers come to be different? . *Earth-Science Reviews*, 114(1–2), 84–107.

Blum, M.D., 2007. Large river systems and climate change. In: Gupta, A. (Ed.), *Large Rivers: Geomorphology and Management*. Wiley, 627–659.

Best, J.L., Ashworth, P.J. (1997). Scour in large braided rivers and the recognition of sequence stratigraphic boundaries. *Nature*, 387, 275–277.

Best, J. (2018). Anthropogenic stresses on the world's big rivers. *Nature Geoscience*, 12, 7–21.

Best J., Darby, S.E., (2020). The Pace of Human-Induced Change in Large Rivers: Stresses, Resilience, and Vulnerability to Extreme Events, *One Earth*, **2**(6), 510–514.

Bombardelli, F.A., Moreno, P.A. (2012). Exchange at the bed sediments-water column interface. In Gualtieri, C., Mihailovic, D.T. (Eds.): Fluid mechanics of environmental interfaces, *CRC Press*, 221-253.

Chanson, H. (2004). *The Hydraulics of Open Channel Flow: An Introduction*. Butterworth-Heinemann, 2nd edition, Oxford, UK, 630 pages

Chaudhry, M.H., 2008. Open Channel Flow.Chaudry, M.H., 2008. Open Channel Flow, 2nd Edition, Springer, Science+Business Media LLC, New York, NY, USA, 524 pages

Getirana, A.C.V., Paiva, R.C.D. (2013), Mapping large-scale river flow hydraulics in the Amazon Basin, *Water Resources Research*, 49, 2437–2445.

Gualtieri, C., Filizola, N., Oliveira, M., Santos, A. M., Ianniruberto, M., (2018). A field study of the confluence between Negro and Solimões Rivers. Part 1: Hydrodynamics and sediment transport. *Comptes Rendus Geoscience*, 350(1−2), January−February 2018, 31−42.

Henderson, F.M. (1966) *Open Channel Flow*. MacMillan Company, New York, USA

Ianniruberto, M., Trevethan, M., Pinheiro, A., Andrade, J.F., Dantas, E., Filizola, N., Santos, A., Gualtieri, C. (2018). A field study of the confluence between Negro and Solimões Rivers. Part 2: River bed morphology and stratigraphy, *Comptes Rendus Geoscience*, 350(1−2), January−February 2018, 43−54.

Gupta, A., 2007. Introduction. In: Gupta (Ed.), Large Rivers: Geomorphology and Management. John Wiley & Sons

Junk, W.J., Bayley, P.B., Sparks, R.E., 1989. The flood pulse concept in river-floodplain systems. In: Dodge, D.P. (Ed.), Proceedings of the International Large River Symposium (LARS). Canadian Special Publications of Fish and Aquatic Sciences, 106, 110–127.

Lane, S., Parsons, D., Best, J., Orfeo, O., Kostaschunk, R., Hardy, R. (2008). Causes of rapid mixing at a junction of two large rivers: Rio Parana and Rio Paraguay, Argentina. *Journal of Geophysical Research*, 113, F02019, 16 pages.

Laraque, A., Moquet, J.S., Alkattam, R., Steiger, J., Mora, A., Adèle, G., Castellanos, B., Lagane, C., López, J.L., Rodriguez, M, Rosales, J. (2013). Seasonal variability of total dissolved fluxes and origin of major dissolved elements within a large tropical river: The Orinoco, Venezuela, *Journal of South American Earth Sciences*, 44, 4-17

Latrubesse, E., Stevaux, J.C., Sinha, R., (2005). Tropical rivers, *Geomorphology*, 70, 187–206

Latrubesse, E.M. (2008). Patterns of anabranching channels: the ultimate end-member adjustments of mega-rivers. *Geomorphology*, 101(1–2), 130–145.

Lewin, J., Ashworth, P.J. (2014). Defining large river channel patterns: Alluvial exchange and plurality, *Geomorphology*, 215, 83–98.

López, J. and Perez-Hernandez, D.: Some Morphological Aspects of the Orinoco River, in: IAHR Symposium on River, Coastal and Estuarine Morphodynamics, Genova, Italy, 6–10 September 1999.

Macklin, M.G., Lewin, J. (2015). The rivers of civilization. *Quaternary Science Review,* 114, 228–244

Meade, R.H., (1994). Suspended sediments of the modern Amazon and Orinoco rivers. In: Iriondo, M. (Ed.), Quaternary of South America, *Quaternary International*, 21, 29– 39.

Mora, A., 2011. Variación temporal y espacial de la concentración de cationes mayoritarios y elementos traza disueltos en el sistema río

Orinoco, Venezuela, Tesis de Doctorado. Escuela Técnica Superior de Ingenieros Industriales. Universidad Politécnica de Madrid. Madrid, España

Nicholas, A.P., Sandbach, S.D., Ashworth, P.J., Amsler, M.L., Best, J.L., Hardy, R.J., Lane, S.N., Orfeo, O., Parsons, D.R., Reesink, A.J.H., Sambrook Smith G.H., Szupiany, R.N. (2012), Modelling hydrodynamics in the Rio Paraná, Argentina: An evaluation and inter-comparison of reduced-complexity and physics based models applied to a large sand-bed river, *Geomorphology*, 169–170, 192–211

Nicholas, A.P., Ashworth, P.J., Sambrook Smith, G.H., Sandbach, S.D. (2013), Numerical simulation of bar and island morphodynamics in anabranching megarivers, *Journal of Geophysical Research: Earth Surface*, 118, 2019–2044.

Nordin Jr., C.F., Perez-Hernandez, D. (1989). Sand waves, bars, and wind-blown sands of the Rı´o Orinoco, Venezuela and Colombia. U. S. Geol. Surv. Water-Supply Pap. 2326A, 74 pp.

Parsons, D.R., Best, J.L., Lane, S.N., Orfeo, O., Hardy, R.J., Kostaschuk, R. (2007). Form roughness and the absence of secondary flow in a large confluence–diffluence, Rio Paraná, Argentina. *Earth Surface Processes and Landforms*, 32(1), 155–162.

RDI, I., 2017. RiverRay ADCP.

Silva León, G., 2005. La cuenca del río Orinoco: visión hidrográfica y balance hídrico (The Orinoco River basin: hydrographic view and its hydrological balance). Revista Geografica Venezolana 46(1): 75−108.

Sime, L., Ferguson, R., Church, M. (2007). Estimating shear stress from moving boat acoustic Doppler measurements in a large gravel bed river. *Water Resources Research*, 43, W03418, 12 pages.

Szupiany, R., Amsler, M., Parsons, D., Best, J. (2009). Morphology, flow structure and suspended bed sediment transport at large braid-bar confluences. *Water Resources Research*, 45, W05415, 19 pages.

Szupiany, R.N., Amsler, M.L., Hernandez, J., Parsons, D.R., Best, J.L., Fornari, F., Trento, A. (2012), Flow fields, bed shear stresses, and suspended bed sediment dynamics in bifurcations of a large river, *Water Resources Research*, 48, W11515, doi:10.1029/2011WR011677.

Trevethan, M., Aoki, S. (2009). Initial observations on relationship between turbulence and suspended sediment properties in Hamana Lake, Japan. *Journal of Coastal Research*, SI (56), 1434-1438.

Wang, B, Xu, Y- J. (2020). Estimating bed material fluxes upstream and downstream of a controlled large bifurcation - the Mississippi- Atchafalaya River diversion. *Hydrological Processes*, 34, 2864–2877

Warne, A.G., Meade, R.H., White, W.A., Guevara, E.H., Gibeaut, J., Smyth, R.C., Aslan, A., Tremblay, T., (2002) Regional controls on geomorphology, hydrology, and ecosystem integrity in the Orinoco Delta, Venezuela, *Geomorphology*, 44, 273–307

Wohl, E.E., 2007. Hydrology of large river basins. In: Gupta, A. (Ed.), Large Rivers: Geomorphology and Management. John Wiley & Sons, 21–44.

Yepez, S.P., Laraque, A., Gualtieri, C., Christophoul, F., Marchan, C., Castellanos, B., Azocar, J.M., Lopez, J.L., Alfonso, J. (2018). Morphodynamic change analysis of bedforms in the Lower Orinoco River, Venezuela, Proceedings IAHS, 377, 41–50

Yuan, S., Tang, H., Hu, L., Xiao, Y., Li, K., Gualtieri, C., Rennie, C.D., Melville, B. (2021). Hydrodynamics, sediment transport and morphological features at the confluence between the Yangtze River and the Poyang Lake, *Water Resources Research*, 57(3), March 2021, e2020WR028284, DOI: 10.1029/2020WR028284

